

1
2
3
4
5
6
7
8
9
10
11
12
13
14
15
16
17
18
19
20
21
22
23
24

Significant contribution of organics to aerosol liquid water content in winter in Beijing, China

Xiaoai Jin¹, Yuying Wang², Zhanqing Li³, Fang Zhang¹, Weiqi Xu^{4,5}, Yele Sun^{4,5}, Xinxin Fan¹, Guangyu Chen⁶, Hao Wu¹, Jingye Ren¹, Qiuyan Wang², and Maureen Cribb³

¹State Key Laboratory of Remote Sensing Science, College of Global Change and Earth System Science, Beijing Normal University, Beijing 100875, China

²Key Laboratory for Aerosol-Cloud-Precipitation of China Meteorological Administration, School of Atmospheric Physics, Nanjing University of Information Science and Technology, Nanjing 210044, China

³Department of Atmospheric and Oceanic Science, and Earth System Science Interdisciplinary Center, University of Maryland, College Park, MD, USA

⁴State Key Laboratory of Atmospheric Boundary Layer Physics and Atmospheric Chemistry, Institute of Atmospheric Physics, Chinese Academy of Sciences, Beijing 100029, China

⁵College of Earth Sciences, University of Chinese Academy of Sciences, Beijing 100049, China

⁶Zhejiang Windey Co., Ltd., Hangzhou 310012, China

Correspondence to: Zhanqing Li (zli@atmos.umd.edu), Yuying Wang (yuyingwang@nuist.edu.cn)

25 **Abstract**

26

27 The aerosol liquid water content (ALWC), an important component of atmospheric particles, has a
28 significant effect on atmospheric optical properties, visibility and multiphase chemical reactions. In
29 this study, ALWC is determined from aerosol hygroscopic growth factor and particle number size
30 distribution (PNSD) measurements and also simulated by the ISORROPIA II thermodynamic model
31 with measured aerosol chemical composition data at an urban site in Beijing from 8 November to 15
32 December 2017. Rich measurements made during the experiment concerning virtually all aerosol
33 properties allow us not only to derive the ALWC but also to study the contributions by various species
34 for which little has been done in this region. The simulated ALWC including the contribution of
35 organics and the calculated ALWC are highly correlated (coefficient of determination $R^2 = 0.92$). The
36 ALWC contributed by organics ($ALWC_{Org}$) accounts for $30 \% \pm 22 \%$ of the total ALWC during the
37 sampling period. These results suggest a significant contribution of organics to ALWC, which is rather
38 different from previous studies that showed negligible contributions by organics. Our results also show
39 that ALWC correlates well with the mass concentrations of sulfate, nitrate, and secondary organic
40 aerosols (SOA) ($R^2 = 0.66, 0.56, \text{ and } 0.60$, respectively). We further noted that accumulation mode
41 particles play a key role in determining ALWC, dominating among all the aerosol modes. ALWC is an
42 exponential function of ambient relative humidity (RH) whose strong diurnal variation influence the
43 diurnal variation of ALWC. However, there is a three-hour lag between the extremes of ALWC and
44 RH values, due to the diurnal variations in PNSD and aerosol chemical composition. Finally, a case
45 study reveals that $ALWC_{Org}$ plays an important role in the formation of secondary aerosols through
46 multiphase reactions at the initial stage of a heavy haze episode.

47

48

49

50 1. Introduction

51 China has experienced rapid economic developments during the past few decades, resulting in
52 frequent heavy haze events. Severe air pollution may harm human health and affect the regional
53 climate through aerosol direct and indirect radiation effects (Li et al., 2016; G. X. Wu et al., 2016; Wei
54 et al., 2019a; Wei et al., 2019b). However, air pollution formation mechanisms and aerosol climate
55 effects remain highly uncertain due to the complex physical and chemical processes involved (Tao et
56 al., 2012; Y. Wang et al., 2014).

57 Aerosol liquid water (ALW), a component of atmospheric particles in the atmosphere, exists
58 universally and plays an important role in many atmospheric physical and chemical processes (Nguyen
59 et al., 2016). For example, ALW can influence aerosol optical properties, resulting in increased
60 extinction coefficients, lowered atmospheric visibilities, enhanced aerosol optical depths (AODs), and
61 changes in the direct climatic effect of aerosols (Dougle et al., 1996; Adams et al., 2001; Liao et al.,
62 2005; Seinfeld and Pandis, 2006). Secondary aerosols (SA) are considered to be the main source of
63 particulate pollution during heavy haze events in China (Huang et al., 2014). Many studies now
64 highlight the significance of aerosol liquid water content (ALWC) in the formation of SA through
65 chemical reactions (e.g., Arellanes et al., 2006; G. Wang et al., 2016; Cheng et al., 2016). This is
66 because ALW can dilute the absolute concentration of solutes, adjust aerosol acidity, and serve as a
67 reactant, resulting in increases in trace gas (e.g., N_2O_5 and HO_2) uptake coefficients (Wahner et al.,
68 1998; Bertram et al., 2009; Abbatt et al., 2012). H. Wang et al. (2017) found that the uptake coefficient
69 of N_2O_5 can be high, which is related to high ALWC in Beijing, thereby increasing the formation of
70 nitrates. ALW can also speed up the aqueous phase chemical reaction by serving as a reactor for the
71 transformation of SO_2 to sulfate (Zheng et al., 2015; G. Wang et al., 2016; Cheng et al., 2016). Some
72 studies have found that ALWC can facilitate the formation of secondary organic aerosols (SOA)
73 through aqueous-phase chemistry and photochemistry (Blando et al., 2001; Surratt et al., 2007;
74 Hennigan et al., 2008; Song et al., 2019). Furthermore, observations in Beijing have shown that

75 aqueous-phase processes play a dominant role in the additional formation of oxidized SOA (Xu et al.,
76 2017). Overall, investigating the formation of SA and haze in North China requires an examination of
77 ALWC and its factors including aerosol particle number size distribution (PNSD), aerosol chemical
78 composition and ambient related humidity (RH) in this region.

79 However, directly measuring real-time ALWC is not feasible yet because of technical limitations,
80 (Kuang et al., 2018). Four indirect methods have been proposed to calculate real-time ALWC: (1) the
81 aerosol PNSD under dry conditions and ambient RH conditions are first measured, then ALWC is
82 calculated as the difference between dry and ambient aerosol volumes (Stanier et al., 2004); (2) the
83 increased aerosol volume due to water uptake (i.e., ALWC) is calculated according to the measured
84 dry PNSD, size-dependent aerosol hygroscopicity, and ambient RH (Kitamori et al., 2009; Bian et al.,
85 2014; Tan et al., 2017); (3) the dry and ambient aerosol volumes are first estimated using the measured
86 aerosol optical enhancement and Ångström exponent, then ALWC is calculated as the difference
87 between dry and ambient aerosol volumes (Kuang et al., 2018); and (4) ALWC is simulated using
88 thermal equilibrium models such as the ISORROPIA thermodynamic model (Nenes et al., 1998),
89 Aerosol Inorganics Model (Wexler and Clegg, 2002), the Simulating Composition of Atmospheric
90 Particles in Equilibrium model (Kim et al., 1993), and the Gibb's Free Energy Minimization model
91 (Ansari et al., 1999) with aerosol chemical composition information as input.

92 ALWC mostly depends on aerosol PNSD, chemical composition, and ambient RH. Hodas et al.
93 (2014) reported that ALWC in the Po Valley in Italy was driven by locally formed anthropogenic
94 nitrates. The implications for the lifetimes of water-soluble organic compounds and its potential
95 influence on SOA formation were also discussed. Another study also revealed that ALWC in Beijing
96 was driven by secondary inorganic aerosols (SIA; Z. Wu et al., 2018). Most previous studies have
97 focused on the interaction between inorganic salts and ALWC, but the impact of organic species on
98 ALWC been ignored to our knowledge (Blando et al., 2001; Surratt et al., 2007; Hennigan et al., 2008;
99 Carlton et al., 2014). A thorough understanding of the association of ALWC with organic aerosols in

100 the atmosphere is lacking.

101 In this study, ALWC is calculated using the indirect method (2) and simulated using the
102 ISORROPIA II model, i.e., indirect method (4), discussed previously. The effects of inorganic aerosols,
103 organic aerosols, PNSD, and ambient RH on ALWC are then investigated separately. We demonstrate
104 the significant contribution of organics to ALWC in Beijing and provide evidence that the ALW
105 contributed by organics serves as a reactor for sulfate and SOA formation.

106 **2. Data and measurements**

107 **2.1. Sampling site**

108 The Air Pollution and Human Health (APHH) winter field campaign took place from 8 November
109 to 15 December 2016 at the Chinese Academy of Sciences' Institute of Atmospheric Physics Tower
110 Branch in Beijing. Beijing is located in the northwest part of the North China Plain, which has
111 experienced rapid economic developments during the last few decades. A large amount of gaseous
112 precursors and other air pollutants are emitted in this region every year, causing serious air pollution
113 problems. The sampling site is located in the northwestern urban area of Beijing (39.97°N, 116.37°E),
114 between the north third and fourth ring roads and surrounded by restaurants. Traffic and cooking
115 emissions are thus the main pollutants at the site. Aerosols at this site can, therefore, well represent
116 anthropogenic aerosols in highly polluted areas. Sun et al. (2013) and Y. Wang et al. (2017) provide
117 more detailed descriptions of the sampling site.

118 **2.2. Instrumentation**

119 Sampling instruments used during the field campaign included a scanning mobility particle sizer
120 (SMPS) equipped with a long differential mobility analyzer (DMA; model 3081A, TSI) and a
121 condensation particle counter (CPC; model 3772, TSI). A custom-built hygroscopicity tandem
122 differential mobility analyzer (H-TDMA) was installed in an air-conditioned mobile container at

123 ground level. The temperature inside the container was maintained at 20–25°C. A high-resolution
124 aerosol mass spectrometer (HR-AMS) was set up in a sampling room located on a two-story roof,
125 about 25 m north from the container. Sampled air went through a PM_{2.5} cyclone inlet fixed on the top
126 of the container before entering the instruments. The RH of the sampled air was dried to below 20 %
127 by a dryer system consisting of a tube filled with silica gel and a Nafion dryer (model PD-70T-24ss,
128 Perma Pure Inc., USA). Various meteorological parameters, including wind speed (WS), wind
129 direction (WD), temperature (*T*), and RH, were measured from a 325-m meteorological tower located
130 ~20 m west of the container. In this study, all times are reported in Beijing local time (UTC+8 h).

131 PNSDs with electrical-mobility diameters ranging from 10 to 600 nm were measured by a
132 scanning mobility particle sizer (SMPS) at a 5-min time resolution. PNSDs were extended to diameters
133 ranging from 0.6 to 1 μm by fitting the measured PNSDs with functions consisting of three-mode log-
134 normal distributions (Hussein et al., 2005). Thus generated are PNSDs with a diameter range of 10 nm
135 to 1 μm.

136 The H-TDMA system developed by the Guangzhou Institute of Tropical and Marine Meteorology
137 measured the size-dependent aerosol hygroscopic growth factor (GF). The H-TDMA system mainly
138 consists of four parts. The first part is a Nafion dryer to keep the RH of sampled air below 20 % and a
139 bipolar neutralizer (soft X-ray, model 3088, TSI Inc.) to equilibrate the particle charge (Wiedensohler
140 et al., 1988). Next, the sampled air passes through the first differential mobility analyzer (DMA1;
141 model 3081L, TSI Inc.) to produce mono-dispersed particles. In this study, the diameters were set to
142 40, 80, 110, 150, and 200 nm. The sampled air then went through a Nafion humidifier (model PD-70T-
143 24ss, Perma Pure Inc., USA) used to humidify the RH of sampled air to 90 %. The last part of the H-
144 TDMA is the second DMA (same model as the DMA1) and a water-based condensation particle
145 counter (model 3787, TSI Inc.), used to measure the number size distribution of humidified particles
146 in the five selected diameters. Y. Wang et al. (2017) provide a detailed introduction to the H-TDMA
147 system.

148 Size-resolved non-refractory sub-micron aerosol chemical species, including organics (Org),
 149 sulfate (SO_4^{2-}), nitrate (NO_3^-), ammonium (NH_4^+), and chloride (Cl^-), were measured by the HR-AMS.
 150 The sampled air dried by diffusion silica gel dryers was drawn into the HR-AMS through a $\text{PM}_{2.5}$
 151 cyclone inlet to remove coarse particles larger than $2.5 \mu\text{m}$. The HR-AMS was calibrated with pure
 152 ammonium nitrate following the procedures detailed in Jimenez et al. (2003). Sun et al. (2016b)
 153 provide operational details about the HR-AMS.

154 3. Method

155 3.1. ALWC calculation based on H-TDMA measurements

156 The ALWC is calculated based on measurements of the aerosol GF and particle number size
 157 distribution. Briefly, H-TDMA data are first used to derive the size-resolved particle GFs at various
 158 RHs. Then ALWC is calculated as the increased aerosol volume due to hygroscopic growth attributed
 159 to water uptake.

160 Chen et al. (2012) showed how to calculate size-resolved particle GFs at different RHs. First, a
 161 three-mode log-normal distribution is applied to fit the measured PNSD to produce fitting parameters
 162 for each mode. The hygroscopicity parameter (κ) in any mode is assumed to be constant. The H-
 163 TDMA-derived size-dependent κ can then be used to deduce the corresponding κ for the nucleation
 164 mode, the Aitken mode, and the accumulation mode of PNSDs according to the following equation:

$$165 \quad \kappa(D_p) = \frac{\sum_{i=1}^3 \kappa_i \cdot N_i(D_p)}{\sum_{i=1}^3 N_i(D_p)}, \quad (1)$$

166 where κ_i refers to the κ of the i th mode, and $N_i(D_p)$ refers to the number concentration of particles in
 167 the i th mode. According to κ -Köhler theory (Petters and Kreidenweis, 2007), κ at a certain diameter
 168 (D_d) can be calculated as

$$169 \quad \kappa(D_d) = (\text{GF}^3 - 1) \cdot \left[\frac{1}{\text{RH}} \exp\left(\frac{4\sigma_s/aM_w}{RT\rho_w D_d \text{GF}}\right) - 1 \right], \quad (2)$$

170 where RH is the control value by the humidifier in the H-TDMA system, T is the mean room

171 temperature of the container set to 293 K, $\sigma_{s/a}$ is the surface tension of the solution/air interface assumed
 172 to be the same as the surface tension coefficient between water and air (about 0.0728 N m⁻¹ at 293 K),
 173 M_w is the molecular weight of water, R is the universal gas constant, ρ_w is the density of water, and D_d
 174 is the diameter of the dry particles. The GF at a given RH is defined as the ratio of the humidified
 175 diameter [D_p (RH)] to D_d :

$$176 \quad \text{GF} = D_p(\text{RH})/D_d . \quad (3)$$

177 The known κ of each mode derives the size-resolved κ at 90 % RH using Eq. (1). Substituting the size-
 178 resolved κ into Eq. (2) results in size-resolved GFs at various RHs. Finally, the volume of ALWC at
 179 ambient RH is equal to the increased aerosol volume due to water uptake, i.e., ALWC can be calculated
 180 as

$$181 \quad \text{ALWC}_{\text{HTDMA}} = \left[\frac{1}{6} \sum_i n_i D_{p,i}^3 \left(\text{GF}(D_{p,i}, \text{RH})^3 - 1 \right) \right] \cdot \rho_w , \quad (4)$$

182 where n_i refers to the particle number concentration of dry particles for the corresponding particle size
 183 range in the i th mode, and $D_{p,i}$ refers to the particle diameter for the corresponding particle size range.

184 **3.2. ALWC simulations based on the ISORROPIA II model**

185 The thermodynamic equilibrium model ISORROPIA II developed by Fountoukis and Nenes
 186 (2007) using aerosol chemical composition information from the HR-AMS can simulate ALWC
 187 (ALWC_{ISO}). The bulk chemical composition was used in the model. However, the ISORROPIA II
 188 model only considers the contribution of inorganic species (Ca^{2+} , K^+ , Mg^{2+} , NH^+ , Na^+ , SO_4^{2-} , NO_3^- ,
 189 Cl^- and H_2O) on ALWC and neglects the contribution of organics. In this study, the model was set up
 190 to reverse mode due to the lack of measurements of gaseous ammonia, and the phase state was assumed
 191 to be stable in the model calculation. As shown in Figure S1, the simulated ALWC in stable mode is
 192 similar to that in metastable mode ($R^2 = 0.99$).

193 According to the model assumptions that the aerosol curvature effect in Köhler theory is ignored,
 194 and the aerosol water uptake has no effect on ambient vapor pressure, the water activity (a_w) defined

195 as the effective mole fraction of water is equal to the ambient RH in this model (Seinfeld and Pandis,
 196 2006):

$$197 \quad a_w = RH \quad (5)$$

198 The ALWC can be calculated using the Zdanovskii–Stokes–Robinson (ZSR) mixing rule (Stokes and
 199 Robinson, 1966),

$$200 \quad ALWC_{ISO} = \sum_i \frac{M_i}{m_{0i}(a_w)}, \quad (6)$$

201 where M_i is the mole concentration of the i th species (mol m^{-3} in air), and $m_{0i}(a_w)$ is the corresponding
 202 molality of the binary solution of the i th species under the same a_w with complex solution. Finally,
 203 with measured ambient RH and T values as input $ALWC_{ISO}$ values under different RH and T conditions
 204 can be derived.

205 3.3. Inferring the contribution of organics to ALWC

206 According to the κ -Köhler theory and the ZSR mixing rule, κ can also be expressed as the sum of
 207 the contributions of each aerosol component:

$$208 \quad \kappa = \sum_i \varepsilon_i \kappa_i, \quad (7)$$

209 where ε_i and κ_i are the volume fraction and hygroscopicity of the i th species, respectively. Submicron
 210 aerosols mainly consist of organic and inorganic species (Carbone et al., 2013; Zieger et al., 2017). As
 211 mentioned in section 2.2, the HR-AMS measures the mass concentrations of organics and inorganics,
 212 including SO_4^{2-} , NO_3^- , NH_4^+ , and Cl^- . The volume fraction of inorganic species can be calculated based
 213 on the ion-pairing scheme given by the following equations (Gysel et al., 2007):

$$214 \quad n_{\text{NH}_4\text{NO}_3} = n_{\text{NO}_3^-},$$

$$215 \quad n_{\text{NH}_4\text{HSO}_4} = \min(2n_{\text{SO}_4^{2-}} - n_{\text{NH}_4^+} + n_{\text{NO}_3^-}, n_{\text{NH}_4^+} - n_{\text{NO}_3^-}),$$

$$216 \quad n_{(\text{NH}_4)_2\text{SO}_4} = \max(n_{\text{NH}_4^+} - n_{\text{NO}_3^-} - n_{\text{SO}_4^{2-}}, 0),$$

$$n_{H_2SO_4} = \max(0, n_{SO_4^{2-}} - n_{NH_4^+} + n_{NO_3^-}),$$

$$n_{HNO_3} = 0, \quad (8)$$

where n represents the mole numbers, and “min” and “max” are minimum and maximum values, respectively. The κ values of the inorganic species sulfuric acid, ammonium sulfate, ammonium hydrogen sulfate, and ammonium nitrate are 1.19, 0.48, 0.56, and 0.58, respectively (Topping et al., 2005; Petters and Kreidenweis, 2007). So the ZSR model can be used to estimate the contribution of inorganic species to the κ value. In this paper, the chloride was not taken into account in ion-pairing because its source is hard to determine. This may result in a minor uncertainty in κ calculation. The hygroscopicity parameter of organics (κ_{Org}) can be calculated using the volume fraction of organics and the total κ value derived from the H-TDMA, according to Eq. (7). Finally, the ALWC contributed by organic species ($ALWC_{Org}$) can be calculated as (Petters and Kreidenweis, 2007)

$$ALWC_{Org} = \frac{m_{Org}\rho_W}{\rho_{Org}} \frac{\kappa_{Org}}{\left(\frac{1}{RH}-1\right)}, \quad (9)$$

where m_{Org} is the organic mass concentration from the AMS (Xu et al., 2015), and ρ_{Org} is the density of organics, taken as 1.4 g cm^{-3} (Moore et al., 2011; Lathem et al., 2013; Cerully et al., 2014).

4. Results and discussion

4.1. Comparison of calculated and simulated ALWC

The trends in ALWC calculated based on the hygroscopic growth factor and PNSD ($ALWC_{HTDMA}$) and simulated from ISOPPOPIA II model ($ALWC_{ISO}$) are generally consistent. Figure 1a shows that $ALWC_{HTDMA}$ and $ALWC_{ISO}$ agree well and that their coefficient of determination (R^2) is 0.89. The correlation is especially strong for RH over 90 %. However, for RH below 60 %, $ALWC_{ISO}$ is less than $ALWC_{HTDMA}$ and even close to 0 in some cases. Bian et al. (2014) and Tan et al. (2017) observed a similar phenomenon in northern and southern China. There are three possible explanations for these results. H-TDMA samples were humidified to 90 % RH during the field campaign, thereby leading to the neglect of the deliquescence process in the $ALWC_{HTDMA}$ calculation. This may lead to

241 overestimation of $ALWC_{HTDMA}$ for RH below the deliquescence relative humidity (DRH). Second, the
242 assumption of constant κ in each mode may lead to small uncertainty in size-resolved GFs at different
243 RHs, resulting in small deviation in ALWC calculation. This may be another reason for the difference
244 between $ALWC_{HTDMA}$ and $ALWC_{ISO}$. In addition, the ISORROPIA II model ignores the effect of
245 aerosol shape and complex organic species on the DRH. Previous studies have suggested that the
246 particle spherical assumption and simplified aerosol chemical species in this model can overestimate
247 the DRH (Seinfeld and Pandis, 2006; Sjogren et al., 2007). So for RH below the simulated DRH
248 (~60 %), particles may still be dry in the ISORROPIA II model, but may have been hydrated in the
249 real atmosphere. Therefore, this model underestimates ALWC. The ambient aerosol deliquescent
250 phenomenon is rare in the North China Plain (Kuang et al., 2016). In addition, the ISORROPIA II
251 model cannot simulate water uptake by organics, which can lead to some bias between simulated and
252 calculated ALWCs. As described in section 3.3, $ALWC_{Org}$ can be inferred and used to discuss
253 differences between $ALWC_{ISO}$ and $ALWC_{HTDMA}$. Figure 1b shows that adding $ALWC_{Org}$ to $ALWC_{ISO}$
254 leads to a stronger correlation with $ALWC_{HTDMA}$ ($R^2 = 0.92$). The correlation improves significantly
255 for RH below 60 %. This demonstrates that (1) organic species contribute significantly to ALWC, and
256 (2) the underestimation of ALWC by the ISORROPIA II model is also related to the neglect of organic
257 species in the model.

258

259 **4.2. Impact of different factors on ALWC**

260 **4.2.1. Impact of aerosol chemical species on ALWC**

261 Figure 2 shows the characteristics of seven heavy pollution events selected for examination.
262 Figures 2a and 2c display the time series of WS, WD, and ambient RH. The prevailing wind during
263 the haze episodes was a weak southerly wind that was favorable for bringing in pollutants from the
264 highly populated and industrialized neighboring regions to the sampling site. This is beneficial to the

265 formation and accumulation of SA (T. Wang et al., 2010; Y. Wang et al., 2017). However, the prevailing
266 winds during the clean events were strong northerly winds that always carried in a clean air mass,
267 resulting in pollutants being quickly removed (Figure 2c). Note that the PM_1 mass concentration
268 decreases somewhat in the evening during haze episodes, following the short-term change of WD from
269 southerly to northerly. This is related to mountain-valley breezes in Beijing (Wehner et al., 2008; Gao
270 et al., 2011; Y. Wang et al., 2017). These results demonstrate that heavy haze episodes have a strong
271 correlation with local wind direction in Beijing.

272 Figures 2a and 2d show the time series of ambient RH and mass concentrations of aerosol chemical
273 species in PM_1 . These figures suggest that the increase in inorganic and organic aerosols is
274 synchronous with the increase in ambient RH during the heavy pollution periods (P1-P7). This is likely
275 because of a positive feedback mechanism driven by Henry's law and thermodynamic equilibrium (Z.
276 Wu et al., 2018). Figure 2b also shows that ALWC continuously increases during the pollution
277 accumulation period. On average, ALWC increases from 8 to $89 \mu g m^{-3}$ as ambient RH increases from
278 15 to 80 %, and the inorganic and organic aerosol mass concentrations increase from 15 to $120 \mu g m^{-3}$
279 and from 12 to $78 \mu g m^{-3}$, respectively. These results imply that the increase in ambient RH and
280 aerosol mass concentration are all important for the increase in ALWC.

281 Equation (4) also suggests that the absolute value of ALWC is dependent on the value of ambient
282 RH and aerosol chemical composition (i.e., the GF value). To further investigate the impact of
283 chemical composition on ALWC, the impact of RH on ALWC should be accounted for. Previous
284 studies suggest there is an exponential relationship between ALWC and RH (e.g., Z. Wu et al., 2018).
285 Here, we define the relative ALWC as the ratio of $ALWC_{HTDMA}$ and the function of ambient RH (e^{bRH}).
286 The b is derived according to the relationship between $ALWC_{HTDMA}$ and RH that is fitted by the
287 function $y = ae^{bx}$. Figure 3a shows the relationship between relative ALWC and primary aerosols
288 (PA) or SA mass concentrations. PA consists of primary organic aerosols (POA) and black carbon
289 (BC), and SA consists of SOA, sulfate, and nitrate. The positive matrix factorization (Paatero and

290 Tapper, 1994) was applied on the organic aerosols (OA) spectral matrices to identify POA and SOA.
291 The relative ALWC is highly correlated with SA mass concentrations ($R^2 = 0.94$) but poorly correlated
292 with PA mass concentrations ($R^2 = 0.69$). High relative ALWCs coincident with high SA mass
293 concentrations suggest that SA plays a key role in the increase in ALWC. This is likely because SA is
294 mainly generated from photochemical reactions in the daytime or reactions at night, making SA highly
295 aged with a hygroscopicity stronger than that of PA (Ervens et al., 2011; Sareen et al., 2017). SA can,
296 therefore, absorb more water vapor than PA in the atmosphere. The enhanced aerosol liquid water
297 induced by SA is further favorable for the formation of SA by speeding up the atmospheric chemical
298 reaction rate and serving as the medium for gas-particle heterogeneous reactions (G. Wang et al., 2016;
299 Cheng et al., 2016). This further increases the bulk aerosol hygroscopicity. This is also the reason why
300 inferred κ based on the ZSR model continuously increases during haze episodes (Figure 2c).

301 Secondary aerosols are mainly composed of nitrate, sulfate, ammonium and SOA. To determine
302 which species is the driver for ALWC in Beijing, Figure 3b shows the correlation analysis between
303 relative ALWC and the mass concentrations of different aerosol chemical species. Relative ALWC and
304 all SIA agree well [R^2 equal to 0.66 (sulfate) and 0.56 (nitrate)]. It has been reported that ALWC is
305 driven by inorganic salts with both nitrate and sulfate playing key roles in determining ALWC (Z. Wu
306 et al., 2018). ALWC also agrees well with SOA ($R^2 = 0.60$) in our study. This is unexpected because
307 the hygroscopicity of SOA is relatively lower than that of nitrate and sulfate. Some studies have also
308 suggested that the water uptake of aged organics accounts for only a few percent of the total aerosol
309 water uptake (e.g., Gysel et al., 2007; Engelhart et al., 2011). In our study, the contribution of $ALWC_{Org}$
310 to total ALWC is significant, accounting for $30 \% \pm 22 \%$. As shown in Figure 4, the contribution of
311 organics to total ALWC varies strongly. This is likely related with the variation in mass fraction and
312 hygroscopicity parameter of organics (κ_{org}). The mass concentration of inorganics increases more than
313 that of organics as RH increases, leading to a lower mass fraction of organics in the case of high
314 ambient RH. Figure 4 also shows $ALWC_{Org}$ fraction increases significantly with the increase of κ_{org} .

315 All these help explain a large variation in the $ALWC_{Org}$ contribution to total ALWC. Considering the
316 distinct ambient RH and κ_{org} between clean and polluted periods, we calculated respectively the
317 fraction of $ALWC_{Org}$ during two periods. There is a higher $ALWC_{Org}$ fraction ($33\% \pm 23\%$) during
318 clean periods than that during polluted periods ($26\% \pm 11\%$). Yet, there is little variability of $ALWC_{Org}$
319 fraction during polluted periods. The larger variability in $ALWC_{Org}$ fraction during clean periods is
320 likely caused by the highly variable κ_{org} when the ambient RH is low. In summary, the contribution of
321 organics in total ALWC varies with the variations of the mass fraction of organics and κ_{org} , and this
322 contribution is significant during both clean and polluted periods. Studies of ALWC in Beijing,
323 therefore, cannot neglect $ALWC_{Org}$. This is different from the studies in other regions such as in the
324 Po Valley in Italy (Hodas et al., 2014) and the eastern U.S. (Carlton et al., 2013) where the ALWC was
325 found to be only driven by nitrate and sulfate respectively.

326 An interesting phenomenon is frequently observed at the initial stage of heavy haze episodes (e.g.,
327 P4, P5, P6, and P7). $ALWC_{ISO}$ is almost close to 0, but both $ALWC_{HTDMA}$ and $ALWC_{Org}$ are always
328 larger than 0, and the organic aerosol mass fraction is high at this stage. These observations reveal that
329 at the initial stage of heavy haze episodes, the ALWC is mostly contributed by organic species.
330 Meanwhile, κ is not very low and increases markedly as the PM_1 mass concentration increases, which
331 is unexpected because of the lower hygroscopicity of organic aerosols compared to SIA. Therefore,
332 some highly hygroscopic substance (i.e., SA) must be generated through multiphase chemical reaction
333 at this stage. We propose that the liquid water contributed by organic species provides a reactor for the
334 transformation of gaseous precursors to SA at the initial stages of heavy haze episodes, increasing the
335 uptake of more liquid water by more SA and further accelerating the formation of heavy haze. Section
336 4.3 provides a case study to demonstrate this.

337 **4.2.2. Impact of PNSD on ALWC**

338 In addition to aerosol chemical composition, ALWC also depends on PNSD (Bian et al., 2014).
339 PNSD does not influence ALWC directly, but it's an important factor to determine the mass

340 concentration and the distribution of hygroscopic materials. As described in section 3.1, the nucleation
341 mode (< 30 nm), the Aitken mode (30–110 nm), and the accumulation mode (110 nm to 1 μ m) (Whitby,
342 1978; Birmili et al., 2001) are considered in this study. Particles with diameters greater than 1 μ m are
343 not considered because some particles in the coarse mode are water soluble but their contribution on
344 the ALWC is low (e.g., Hussein et al., 2004; S. Liu et al., 2008; Bian et al., 2014; Tan et al., 2017).

345 The contributions of nucleation mode, Aitken mode, and accumulation mode particles to
346 $ALWC_{HTDMA}$ are about 1.0 %, 18.0 %, and 82.0 %, respectively. Figure 5 shows the correlations
347 between $ALWC_{HTDMA}$ and the volume concentrations of different mode particles, and the average
348 contribution of different mode particles to $ALWC_{HTDMA}$ (f_{ALWC}) under five different RH conditions.
349 The R^2 and f_{ALWC} of the nucleation mode particles (left column in Figure 5) are all less than 0.1 and
350 1 %, respectively, under all RH conditions. This is likely because the volume concentration of
351 nucleation mode particles is very low, and most of these small particles are composed of hydrophobic
352 chemical species such as BC and POA. Similarly, the number concentration of Aitken mode particles
353 also shows weak correlations with $ALWC_{HTDMA}$ ($R^2 < 0.2$) under $RH < 90$ % conditions, but their
354 correlation ($R^2 = 0.25$) is enhanced significantly under $RH > 90$ % conditions (middle column of Figure
355 5). This is because there are more aged particles in the Aitken mode which can absorb much more
356 water when the ambient RH is higher than 90 %. However, the contribution of the Aitken mode to
357 ALWC ranges from 14 % to 21 % and decreases as RH increases. $ALWC_{HTDMA}$ is strongly correlated
358 to the volume concentration of accumulation mode particles, with R^2 and f_{ALWC} greater than 0.6 and
359 75 %, respectively, under all RH conditions (right column of Figure 5). Figure 5 also shows that ALWC
360 increases slightly as the volume concentration of accumulation mode particles increases under $RH <$
361 70 % conditions (slope < 0.001), but increases strongly under higher RH conditions, especially under
362 $RH > 90$ % conditions (slope = 0.0041). This is likely because there are more accumulation mode SA
363 formed due to multiphase chemical reactions under high ambient RH conditions. Swietlicki et al.
364 (1999) have suggested that the contribution of accumulation mode particles to ALWC is largest for all-

365 mode particles.

366 In summary, the contribution of nucleation mode particles to ALWC is very low. The contribution
367 of Aitken mode particles is much higher than nucleation mode particles and decreases with increasing
368 ambient RH. The contribution of accumulation mode particles to ALWC is largest under all RH
369 conditions and increases with increasing ambient RH, thus playing a key role in determining ALWC.

370 **4.2.3. Impact of RH on ALWC**

371 As discussed in 4.2.1, the absolute value of ALWC has an exponential relationship with ambient
372 RH. Figure 6 shows the relationship between ALWC and RH for different PM₁ mass concentration
373 ranges. ALWC increases slowly as RH increases under lower ambient RH conditions then sharply
374 increases when RH exceeds a critical RH value. This critical RH value is different for different PM₁
375 mass concentrations. This is because the low RH conditions cannot provide enough water for aerosol
376 particles, even though the PNSD is dominated by accumulation mode particles with higher
377 hygroscopicity (Tan et al., 2016). This demonstrates the important influence of RH on ALWC. The
378 lower critical RH value for higher PM₁ mass concentrations (~80 %) suggests that ALWC is easily
379 formed under heavily polluted conditions. This is likely because there are more SA and accumulation
380 mode particles during pollution periods (Sun et al., 2016a; Y. Wang et al., 2017).

381 Figure 7a shows the diurnal variations of ALWC_{HTDMA} and ambient RH during the sampling
382 period. The extreme ALWC_{HTDMA} values appear at night and during the day respectively, likely related
383 to the diurnal variations of ambient RH. The elevated ambient RH at night not only increases ALWC
384 through water uptake of particles directly, but also facilitates the formation of hydrophilic particulate
385 nitrate through the speeding up of the uptake coefficient of N₂O₅ (Thornton et al., 2003; Bertram et
386 al., 2009). This can further enhance ALWC. However, although the diurnal variations of ALWC_{HTDMA}
387 and ambient RH are similar, the peak and nadir of ALWC_{HTDMA} (0300 LT and 1100 LT, respectively)
388 appear three hours earlier than the peak and nadir of ambient RH (0600 LT and 1400 LT, respectively).
389 This time difference is likely related to changes in PNSD. The diurnal variation of PNSD (Figure 7b)

390 shows that the number concentrations of Aitken and accumulation mode particles begin to decrease
391 quickly at 0300 LT. ALWC also begins to decrease, although the ambient RH increases slightly at that
392 time. In the morning, ALWC decreases sharply following the ambient RH and PNSD changes due to
393 the lifting planetary boundary layer height. ALWC decreases to its minimum value at ~1100 LT then
394 begins to increase quickly. However, ambient RH still decreases at that time and reaches its minimum
395 value at ~1400 LT. The increase in ALWC is likely associated with changes in aerosol chemical species
396 and PNSD. Figure 7b and 7c show that there are many newly formed Aitken and accumulation mode
397 particles and that the fraction of SA increases at noon, likely because of strong photochemical
398 reactions. Y. Wang et al. (2017, 2018) have suggested that daytime photochemical reactions are
399 efficient enough to enhance aerosol hygroscopicity and change the aerosol mixing state from external
400 to internal in North China through the formation of hydrophilic chemical species. All this suggests that
401 ambient RH is not the only determining factor for ALWC. PNSD and aerosol chemical composition
402 are also important for ALWC.

403 **4.3. A case study of the impact of $ALWC_{Org}$ on SA formation**

404 As discussed in section 4.2.1, a hypothesis is proposed that $ALWC_{Org}$ maybe provide a reactor for
405 the formation of secondary species. To verify this hypothesis, the P4 case shown in Figure2 is selected
406 to further analyze the influence of $ALWC_{Org}$ on the formation of secondary aerosols (Figure 8). Figure
407 8a shows the time series of $ALWC_{HTDMA}$, $ALWC_{ISO}$, and $ALWC_{Org}$ during this case. On 27 November
408 2017, $ALWC_{ISO}$ was close to 0 all day long because of the low ambient RH, but both $ALWC_{HTDMA}$ and
409 $ALWC_{Org}$ were always larger than 0, increasing with increasing PM_{10} mass concentration (Figure 8a).
410 Figure 8a also shows that the fraction of $ALWC_{Org}$ in $ALWC_{HTDMA}$ was high at the initial stage of this
411 pollution case, but this fraction decreased as haze increased. This case was further divided into three
412 periods (Figure 8b). Organics were the most abundant chemical species during the first period (64 %),
413 which explains the high fraction of $ALWC_{Org}$ in $ALWC_{HTDMA}$ at the initial stage of this haze case. The
414 pie charts in Figure 8b also show that both SOA and SIA (sulfate, nitrate, and ammonium) increases

415 from the first to third periods but POA decreases, likely related to multiphase reactions (i.e., aqueous-
416 phase reactions) due to the enhanced ALWC. Time series of f_{44} and the fraction of sulfate in total sulfur
417 ($F_{\text{SO}_4^{2-}}$) are also shown to further illustrate the influence of aqueous-phase reactions on aerosol
418 chemical species. The m/z 44 signal intensity f_{44} (mostly contributed by the CO_2^+ ion) measured by the
419 AMS can be used as an indicator of the oxidation level in organic species (Mei et al., 2013). The sulfur
420 oxidation ratio $F_{\text{SO}_4^{2-}}$ (Sun et al., 2006) is defined as

$$421 \quad F_{\text{SO}_4^{2-}} = \frac{n[\text{SO}_4^{2-}]}{n[\text{SO}_4^{2-}] + n[\text{SO}_2]}, \quad (10)$$

422 where $n[\text{SO}_4^{2-}]$ and $n[\text{SO}_2]$ refer to the molar concentrations of SO_4^{2-} and SO_2 , respectively. Figure 8b
423 suggests that f_{44} and $F_{\text{SO}_4^{2-}}$ both increase gradually with increasing $\text{ALWC}_{\text{HTDMA}}$ and PM_{10} mass
424 concentration from 27 November to 30 November 2017. This is likely because the increase in ALWC
425 is beneficial to the oxidation of organics and the transformation of SO_2 to SO_4^{2-} , implying the
426 importance of aqueous-phase chemical reaction on haze formation in Beijing. The production of
427 secondary organic and inorganic species can further enhance aerosol hygroscopicity, increasing ALWC
428 in the atmosphere. This positive feedback is the reason behind the rapid formation of heavy haze events
429 in Beijing (G. Wang et al., 2016). A rapid increase in f_{44} and $F_{\text{SO}_4^{2-}}$ was seen during the first period at
430 night on 27 November (shown by green and red arrows in Fig. 8) when organics contributed the most
431 to ALWC. This suggests that ALWC contributed by organics may have played an important role in the
432 formation of secondary species at the initial stage of the pollution event.

433

434 5. Conclusions

435 In this study, the aerosol liquid water content (ALWC) was calculated using the size-resolved
436 aerosol hygroscopic growth factor and the particle number size distribution (PNSD) measured at a
437 Beijing urban site during the APHH winter campaign (8 November to 15 December 2017). Also done

438 were simulations using the ISORROPIA II model with measured aerosol chemical composition data
439 as input data. During the sampling period, seven heavy haze episodes were selected to investigate the
440 influence of different factors (PNSD, ambient RH, and aerosol chemical composition) on ALWC.

441 The calculated and simulated ALWC ($ALWC_{HTDMA}$ and $ALWC_{ISO}$) agree well (correlation of
442 determination R^2 equal to 0.89). However, $ALWC_{ISO}$ is much lower than $ALWC_{HTDMA}$ for RH below
443 60 %, even approaching zero many times. This deviation is in part attributed to the neglect of the
444 contribution of organics to ALWC ($ALWC_{Org}$) in the ISORROPIA II model, contradicting with
445 previous studies ignoring this contribution. The aerosol hygroscopicity of organics was also derived
446 in this study for use in calculating $ALWC_{Org}$. The sum of $ALWC_{ISO}$ and $ALWC_{Org}$ has a higher
447 correlation ($R^2 = 0.92$) with the calculated ALWC (i.e., $ALWC_{HTDMA}$), especially for RH below 60 %.
448 This implies that organic aerosols are also an important contributor to ALWC.

449 PNSD, ambient RH, and aerosol chemical composition are all found to affect ALWC significantly.
450 Nucleation mode and Aitken mode particles have little influence on ALWC. Accumulation mode
451 particles play a key role in determining ALWC and dominate among all aerosol modes. ALWC is
452 highly related to the relative humidity (RH) when RH exceeds a critical RH value that is different for
453 different PM_{10} mass concentrations. ALWC varies diurnally with its extreme values appearing at night
454 and during the day respectively. The diurnal variation of ambient RH explains this. However, there is
455 a three-hour difference between when the extreme ALWC and RH values occur, caused by the diurnal
456 variations in PNSD and aerosol chemical composition.

457 On average, $ALWC_{Org}$ accounts for $\sim 30 \% \pm 22 \%$ of the total aerosol liquid water during the
458 sampling period. This shows the significant contribution of organic species to ALWC. Our results
459 suggest that ALWC is not only driven by inorganic salts but also driven by organics in Beijing. This is
460 different from the results obtained in the Po Valley in Italy (Hodas et al., 2014) and the eastern U.S.
461 (Carlton et al., 2013) where the ALWC is driven by nitrate and sulfate respectively. Finally, one case
462 study was used to study the importance of $ALWC_{Org}$ on multiphase chemical reactions. $ALWC_{Org}$ was

463 found to play an important role in the formation of secondary aerosols by speeding up aqueous-phase
464 reactions at the initial stage of heavy haze. Our study is important for investigating the contribution of
465 organics to ALWC and its importance on haze formation in Beijing.

466

467 *Data availability.* Data used in the study are available from the first author upon request
468 (201631490012@mali.bnu.edu.cn).

469

470 *Author contributions.* ZL and YW designed the experiment; YW, XJ, and WX carried it out and
471 analyzed the data; other co-authors participated in science discussions and suggested additional
472 analyses. XJ and YW prepared the paper with contributions from all co-authors.

473

474 *Competing interests.* The authors declare no competing interests.

475

476 *Acknowledgements.* This work was funded by the National Key R&D Program of China (grant no.
477 2017YFC1501702), the National Natural Science Foundation of China (NSFC) research projects
478 (grant nos. 91544217, 41575132, 41675141, 41705125), the Startup Foundation for Introducing Talent
479 of NUIST and the National Basic Research Program of China “973” (grant no. 2013CB955801). We
480 thank all participants of the field campaign for their tireless work and cooperation.

481

482 **References**

483

484 Abbatt, J. P. D., Lee, A. K. Y., Thornton, J. A.: Quantifying Trace Gas Uptake to Tropospheric Aerosol:
485 Recent Advances and Remaining Challenges, *Chem. Soc. Rev.*, 41(19), 6555–6581,
486 <https://doi.org/10.1039/c2cs35052a>, 2012.

487 Adams, P. J., and Seinfeld, J. H.: General circulation model assessment of direct radiative forcing by
488 the sulfate-nitrate–ammonium–water inorganic aerosol system, *J. Geophys. Res.-Atmos.*, 106,
489 1097–1111, <https://doi.org/10.1029/2000JD900512>, 2001.

490 Ansari, A.S., Pandis, S.N.: Prediction of multicomponent inorganic atmospheric aerosol behavior,
491 *Atmos. Environ.*, 33 (5), 745–757, [https://doi.org/10.1016/S1352-2310\(98\)00221-0](https://doi.org/10.1016/S1352-2310(98)00221-0), 1999.

492 Arellanes, C., Paulson, S. E., Fine, P. M., and Sioutas, C.: Exceeding of Henry’s Law by Hydrogen
493 Peroxide Associated with Urban Aerosols, *Environ. Sci. Technol.*, 40, 4859–4866,
494 <https://doi.org/10.1021/es0513786>, 2006.

495 Bertram, T. H., Thornton, J. A.: Toward a general parameterization of N₂O₅ reactivity on aqueous
496 particles: the competing effects of particle liquid water, nitrate and chloride, *Atmos. Chem. Phys.*, 9
497 (21), 8351–8363, <https://doi.org/10.5194/acp-9-8351-2009>, 2009.

498 Bian, Y.X., Zhao, C.S., Ma, N., Chen, J., Xu, W.Y.: A study of aerosol liquid water content based on
499 hygroscopicity measurements at high relative humidity in the North China Plain, *Atmos. Chem.*
500 *Phys.*, 14 (12), 6417–6426, <https://doi.org/10.5194/acp-14-6417-2014>, 2014.

501 Birmili, W., Wiedensohler, A., Heintzenberg, J., and Lehmann, K.: Atmospheric particle number size
502 distribution in central Europe: Statistical relations to air masses and meteorology, *J. Geophys. Res.-*
503 *Atmos.*, 106, 32005–32018, <https://doi.org/10.1029/2000JD000220>, 2001.

504 Blando, J. D., Turpin, B. J.: Secondary organic aerosol formation in cloud and fog droplets: a literature
505 evaluation of plausibility, *Atmos. Environ.*, 34, 1623–1632, [https://doi.org/10.1016/S1352-
506 *2310\(99\)00392-1*, 2001.](https://doi.org/10.1016/S1352-2310(99)00392-1)

507 Carbone, S., Saarikoski, S., Frey, A., Reyes, F., Reyes, P., Castillo, M., Gramsch, E., Oyola, P., Jayne,
508 J., Worsnop, DR., and Hillamo, R.: Chemical characterization of submicron aerosol particles in
509 Santiago de Chile, *Aerosol Air Qual. Res.*, 13(2), 462-473,
510 <https://doi.org/10.4209/aaqr.2012.10.0261>, 2013.

511 Carlton, A. G., Turpin, B. J.: Particle partitioning potential of organic compounds is highest in the
512 Eastern US and driven by anthropogenic water, *Atmos. Chem. Phys.*, 13 (20), 10203–10214,
513 <https://doi.org/10.5194/acp-13-10203-2013>, 2013.

514 Cerully, K. M., Bougiatioti, A., Hite Jr., J. R., Guo, H., Xu, L., Ng, N. L., Weber, R., and Nenes, A.:
515 On the link between hygroscopicity, volatility, and oxidation state of ambient and water-soluble
516 aerosol in the Southeastern United States, *Atmos. Chem. Phys.*, 14, 30835–30877,
517 <https://doi.org/10.5194/acpd-14-30835-2014>, 2014.

518 Chen, J., Zhao, C. S., Ma, N., Liu, P. F., Göbel, T., Hallbauer, E., Deng, Z. Z., Ran, L., Xu, W. Y.,
519 Liang, Z., Liu, H. J., Yan, P., Zhou, X. J., and Wiedensohler, A.: A parameterization of low visibilities
520 for hazy days in the North China Plain, *Atmos. Chem. Phys.*, 12, 4935–4950,
521 <https://doi.org/10.5194/acp-12-4935-2012>, 2012.

522 Cheng, Y., Zheng, G., Wei, C., Mu, Q., Zheng, B., Wang, Z., Gao, M., Zhang, Q., He, K., Carmichael,
523 G., Pöschl, U., Su, H.: Reactive nitrogen chemistry in aerosol water as a source of sulfate during

524 haze events in China, *Sci. Adv.*, 2 (12), e1601530, <https://doi.org/10.1126/sciadv.1601530>, 2016.

525 Dougle, P. G., Vlasenko, A. L., Veefkind, J. P., and Brink, H. M. T.: Humidity dependence of the light
526 scattering by mixtures of ammonium nitrate, ammonium sulfate and soot, *J. Aerosol. Sci.*, 27, 513–
527 514, [https://doi.org/10.1016/0021-8502\(96\)00329-1](https://doi.org/10.1016/0021-8502(96)00329-1), 1996.

528 Engelhart, G.J., Hildebrandt, L., Kostenidou, E., Mihalopoulos, N., Donahue, N.M., Pandis, S.N.:
529 Water content of aged aerosol, *Atmos. Chem. Phys.*, 11, 911–920, [https://doi.org/10.5194/acp-11-](https://doi.org/10.5194/acp-11-911-2011)
530 911-2011, 2011.

531 Ervens, B., Turpin, B. J., Weber, R. J.: Secondary organic aerosol formation in cloud droplets and
532 aqueous particles (aqSOA): a review of laboratory, field and model studies, *Atmos. Chem. Phys.*,
533 11 (21), 11069–11102, <https://doi.org/10.5194/acp-11-11069-2011>, 2011.

534 Fountoukis, C. and Nenes, A.: ISORROPIA II: a computationally efficient thermodynamic equilibrium
535 model for K^+ – Ca^{2+} – Mg^{2+} – NH_4^+ – Na^+ – $SONO$ – Cl^- – H_2O aerosols, *Atmos. Chem. Phys.*, 7, 4639–
536 4659, <https://doi.org/10.5194/acp-7-4639-2007>, 2007.

537 Gao, Y., Liu, X., Zhao, C., and Zhang, M.: Emission controls versus meteorological conditions in
538 determining aerosol concentrations in Beijing during the 2008 Olympic Games, *Atmos. Chem.*
539 *Phys.*, 11, 12437–12451, <https://doi.org/10.5194/acp-11-12437-2011>, 2011.

540 Gysel, M., Grosier, J., Topping, D.O., Whitehead, J.D., Bower, J.N., Cubison, M.J., Williams, P.I.,
541 Flynn, M.J., McFiggans, G.B., Coe, H.: Closure study between chemical composition and
542 hygroscopic growth of aerosol particles during TORCH2, *Atmos. Chem. Phys.*, 7 (24), 6131–6144,
543 <https://doi.org/10.5194/acp-7-6131-2007>, 2007.

544 Hennigan, C. J., Bergin, M. H., Dibb, J. E., Weber, R. J.: Enhanced secondary organic aerosol
545 formation due to water uptake by fine particles, *Geophys. Res. Lett.*, 35(18), No. L18801,
546 <https://doi.org/10.1029/2008GL035046>, 2008.

547 Hodas, N., Sullivan, A. P., Skog, K., Keutsch, F. N., Collett, J. L., Decesari, S., Facchini, M. C.,
548 Carlton, A. G., Laaksonen, A., Turpin, B. J.: Aerosol Liquid Water Driven by Anthropogenic Nitrate:
549 Implications for Lifetimes of Water-Soluble Organic Gases and Potential for Secondary Organic
550 Aerosol Formation, *Environ. Sci. Technol.*, 48 (19), 11127–11136
551 <https://doi.org/10.1021/es5025096>, 2014.

552 Huang, R., Zhang, Y., Bozzetti, C., Ho, K., Cao, J., Han, Y., Daellenbach, K. R., Slowik, J. G., Platt,
553 S. M., Canonaco, F.: High secondary aerosol contribution to particulate pollution during haze events
554 in China, *Nature.*, 514 (7521), 218, <https://doi.org/10.1038/nature13774>, 2014,.

555 Hussein, T., Puustinen, A., Aalto, P. P., Mäkelä, J. M., Hämeri, K., and Kulmala, M.: Urban aerosol
556 number size distributions, *Atmos. Chem. Phys.*, 4, 391–411, [22](https://doi.org/10.5194/acp-4-391-</p></div><div data-bbox=)

557 2004, 2004.

558 Hussein, T., Dal Maso, M., Petäjä, T., Koponen, I. K., Paatero, P., Aalto, P. P., Hämeri, K., and Kulmala,
559 M.: Evaluation of an automatic algorithm for fitting the particle number size distributions, *Boreal*
560 *Environ. Res.*, 10, 337–355, 2005.

561 Jimenez, J. L., Jayne, J. T., Shi, Q., Kolb, C. E., Worsnop, D. R., Yourshaw, I., Morris, J. W.: Ambient
562 aerosol sampling using the aerodyne aerosol mass spectrometer, *J. Geophys. Res.-Atmos.*, 108(D7),
563 [https://doi.org/ https://doi.org/10.1029/2001JD001213](https://doi.org/10.1029/2001JD001213), 2003.

564 Kim, Y.P., Seinfeld, J.H., Saxena, P.: Atmospheric gas-aerosol equilibrium I. Thermodynamic model,
565 *Aerosol Sci. Technol.*, 19 (2), 157–181, <https://doi.org/10.1080/02786829308959628>, 1993.

566 Kitamori, Y., Mochida, M., Kawamura, K.: Assessment of the aerosol water content in urban
567 atmospheric particles by the hygroscopic growth measurements in Sapporo, Japan. *Atmos. Environ.*,
568 43 (21), 3416–3423, <https://doi.org/10.1016/j.atmosenv.2009.03.037>, 2009.

569 Kuang Y., Zhao C.S., Ma N., Liu H.J., Bian Y.X., Tao J.C. and Hu M.: Deliquescent phenomena of
570 ambient aerosols on the North China Plain, *Geophys Res Lett*, 43, 8744-8750,
571 <https://doi.org/10.1002/2016GL070273>, 2016.

572 Kuang, Y., Zhao, C. S., Zhao, G., Tao, J. C., Xu, W., Ma, N., and Bian, Y. X.: A novel method for
573 calculating ambient aerosol liquid water content based on measurements of a humidified
574 nephelometer system, *Atmospheric Measurement Techniques*, 11(5), 2967-2982,
575 <https://doi.org/10.5194/amt-11-2967-2018>, 2018.

576 Latham, T. L., Beyersdorf, A. J., Thornhill, K. L., Winstead, E. L., Cubison, M. J., Hecobian, A.,
577 Jimenez, J. L., Weber, R. J., Anderson, B. E., and Nenes, A.: Analysis of CCN activity of Arctic
578 aerosol and Canadian biomass burning during summer 2008, *Atmos. Chem. Phys.*, 13, 2735–2756,
579 <https://doi.org/10.5194/acp-13-2735-2013>, 2013.

580 Liao, H., Seinfeld, J. H.: Global impacts of gas-phase chemistry aerosol interactions on direct radiative
581 forcing by anthropogenic aerosols and ozone, *J. Geophys. Res.-Atmos.*, 110 (D18).
582 <https://doi.org/10.1029/2005JD005907>, 2005.

583 Li, Z., Lau, W. M., Ramanathan, V., Wu, G., Ding, Y., Manoj, M. G., Liu, J., Qian, Y., Li, J., and Zhou,
584 T.: Aerosol and mon- soon climate interactions over Asia, *Rev. Geophys.*, 54, 866–929,
585 <https://doi.org/10.1002/2015RG000500>, 2016.

586 Liu, S., Hu, M., Wu, Z., Wehner, B., Wiedensohler, A., and Cheng, Y.: Aerosol number size distribution
587 and new particle formation at a rural/coastal site in Pearl River Delta (PRD) of China, *Atmos.*
588 *Environ.*, 42, 6275–6283, <https://doi.org/10.1016/j.atmosenv.2008.01.063>, 2008.

589 Mei F., Setyan A., Zhang Q. and Wang J.: CCN activity of organic aerosols observed downwind of
590 urban emissions during CARES, *Atmos. Chem. Phys.*, 13, 12155-12169,

591 <https://doi.org/10.5194/acp-13-12155-2013>, 2013.

592 Moore, R. H., Bahreini, R., Brock, C. A., Froyd, K. D., Cozic, J., Holloway, J. S., Middlebrook, A. M.,
593 Murphy, D. M., and Nenes, A.: Hygroscopicity and composition of Alaskan Arctic CCN during
594 April 2008, *Atmos. Chem. Phys.*, 11, 11807–11825, <https://doi.org/10.5194/acp-11-11807-2011>,
595 2011.

596 Nenes, A., Pandis, S.N., Pilinis, C.: ISORROPIA: a new thermodynamic equilibrium model for
597 multiphase multicomponent inorganic aerosols, *Aquat. Geochem.*, 4 (1), 123–152,
598 <https://doi.org/10.1023/A:1009604003981>, 1998.

599 Nguyen, T. K. V., Zhang, Q., Jimenez, J. L., Pike, M., Carlton, A. G.: Liquid Water: Ubiquitous
600 Contributor to Aerosol Mass, *Environ. Sci. Technol. Lett.*, 3 (7), 257–263,
601 <https://doi.org/10.1021/acs.estlett.6b00167>, 2016.

602 Paatero, P., & Tapper, U. (2010). Positive matrix factorization: a non-negative factor model with
603 optimal utilization of error estimates of data values. *Environmetrics*, 5(2), 111-126.

604 Petters, M. D. and Kreidenweis, S. M.: A single parameter representation of hygroscopic growth and
605 cloud condensation nucleus activity, *Atmos. Chem. Phys.*, 7, 1961–1971,
606 <https://doi.org/10.5194/acp-7-1961-2007>, 2007.

607 Sareen, N., Waxman, E. M., Turpin, B. J., Volkamer, R., Carlton, A. G.: Potential of Aerosol Liquid
608 Water to Facilitate Organic Aerosol Formation: Assessing Knowledge Gaps about Precursors and
609 Partitioning, *Environ. Sci. Technol.*, 51 (6), 3327–3335, <https://doi.org/10.1021/acs.est.6b04540>,
610 2017.

611 Seinfeld, H. J., Pandis, N. S.: *Atmospheric Chemistry and Physics: From Air Pollution to Climate*
612 *Change*, Taylor & Francis Group, <https://doi.org/10.1080/00139157.1999.10544295>, 2006.

613 Sjogren, S., Gysel, M., Weingartner, E., Baltensperger, U., Cubison, M. J., Coe, H., Zardini, A. A.,
614 Marcolli, C., Krieger, U. K., and Peter, T.: Hygroscopic growth and water uptake kinetics of two-
615 phase aerosol particles consisting of ammonium sulfate, adipic and humic acid mixtures, *J. Aerosol*
616 *Sci.*, 38, 157–171, <https://doi.org/10.1016/j.jaerosci.2006.11.005>, 2007.

617 Song, S., Gao, M., Xu, W., et al.: Possible heterogeneous chemistry of hydroxyl-methane-sulfonate
618 (HMS) in northern China winter haze, *Atmos. Chem. Phys.*, 19(2): 1357-1371,
619 <https://doi.org/10.5194/acp-19-1357-2019>, 2019.

620 Stanier, C.O., Khlystov, A.Y., Chan, W.R., Mandiro, M., Pandis, S.N.: A method for the in situ
621 measurement of fine aerosol water content of ambient aerosols: The Dry Ambient Aerosol Size
622 Spectrometer (DAASS), *Aerosol Sci. Technol.*, 38 (1), 215–228,
623 <https://doi.org/10.1080/02786820390229525>, 2004.

624 Stokes, R. H. and Robinson, R. A.: Interactions in aqueous nonelectrolyte solutions. I. Solute-solvent

625 equilibria, *J. Phys. Chem.*, 70, 2126–2131, <https://doi.org/10.1021/j100879a010>, 1966.

626 Sun, Y., Zhuang, G., Tang, A., Wang, Y., An, Z.: Chemical characteristics of PM_{2.5} and PM₁₀ in haze-
627 fog episodes in Beijing, *Environ. Sci. Technol.*, 40, 3148-3155, <https://doi.org/10.1021/es051533g>,
628 2006.

629 Sun, Y., Z. F. Wang, P. Q. Fu, T. Yang, Q. Jiang, H. B. Dong, J. Li, and J. J. Jia.: Aerosol composition,
630 sources and processes during wintertime in Beijing, China, *Atmos. Chem. Phys.*, 13(9), 4577–4592,
631 <https://doi.org/10.5194/acp-13-4577-2013>, 2013.

632 Sun Y., Chen C., Zhang Y., Xu W., Zhou L., Cheng X., Zheng H., Ji D., Jie L. and Xiao T.: Rapid
633 formation and evolution of an extreme haze episode in Northern China during winter 2015, *Sci.*
634 *Rep.*, 6(1):27151, <https://doi.org/10.1038/srep27151>, 2016a.

635 Sun, Y., Wang, Z., Wild, O., Xu, W., Chen, C., Fu, P., Du, W., Zhou, L., Zhang, Q., and Han, T.: “APEC
636 Blue”: Secondary Aerosol Reductions from Emission Controls in Beijing, *Sci. Rep.*, 6, 20668,
637 <https://doi.org/10.1038/srep20668>, 2016b.

638 Surratt, J. D., Kroll, J. H., Kleindienst, T. E., Edney, E. O., Claeys, M., Sorooshian, A., Ng, N. L.,
639 Offenberg, J. H., Lewandowski, M., Jaoui, M., Flagan, R. C., Seinfeld, J. H.: Evidence for
640 organosulfates in secondary organic aerosol, *Environ. Sci. Technol.*, 41, 517–527,
641 <https://doi.org/10.1021/es062081q>, 2007.

642 Swietlicki, E., Zhou, J., Berg, O. H., Martinsson, B. G., Frank, G., Cederfelt, S. I., Dusek, U., Berner,
643 A., Birmili, W., Wiedensohler, A., Yuskiewicz, B., and Bower, K. N.: A closure study of sub-
644 micrometer aerosol particle hygroscopic behaviour, *Atmos. Res.*, 50, 205–240,
645 [https://doi.org/10.1016/S0169-8095\(98\)00105-7](https://doi.org/10.1016/S0169-8095(98)00105-7), 1999.

646 Tan, H., Cai, M., Fan, Q., Liu, L., Li, F., & Chan, P. W., et al.: An analysis of aerosol liquid water
647 content and related impact factors in pearl river delta, *Science of The Total Environment*, 579, 1822-
648 1830, <https://doi.org/10.1016/j.scitotenv.2016.11.167>, 2017.

649 Tao, W. K., Chen, J. P., Li, Z., Wang, C., and Zhang, C.: Impact of Aerosols on Convective Clouds and
650 Precipitation, *Rev. Geo. phys.*, 50, 1–62, <https://doi.org/10.1029/2011RG000369>, 2012.

651 Thornton, J. A., Braban, C. F., Abbatt, J. P. D.: N₂O₅ hydrolysis on sub-micron organic aerosols: the
652 effect of relative humidity, particle phase, and particle size. *Atmos. Chem. Phys.*, 5 (20), 4593–4603,
653 <https://doi.org/10.1039/b307498f>, 2003.

654 Topping D O, Mcfiggans G B, Coe H.: A curved multi-component aerosol hygroscopicity model
655 framework: Part 1 – Inorganic compounds, *Atmos. Chem. Phys.*, 5(5): 1205-1222,
656 <https://doi.org/10.5194/acp-5-1205-2005>, 2005.

657 Wahner, A., Mentel, T. F., Sohn, M., Stier, J.: Heterogeneous reaction of N₂O₅ on sodium nitrate

658 aerosol, *J. Geophys. Res. Atmos.*, 103 (D23), 31103–31112, <https://doi.org/10.1029/1998JD100022>,
659 1998.

660 Wang, G., Zhang, R., Gomez, M. E., Yang, L., Levy Zamora, M., Hu, M., Lin, Y., Peng, J., Guo, S.,
661 Meng, J., Li, J., Cheng, C., Hu, T., Ren, Y., Wang, Y., Gao, J., Cao, J., An, Z., Zhou, W., Li, G.,
662 Wang, J., Tian, P., MarreroOrtiz, W., Secrest, J., Du, Z., Zheng, J., Shang, D., Zeng, L., Shao, M.,
663 Wang, W., Huang, Y., Wang, Y., Zhu, Y., Li, Y., Hu, J., Pan, B., Cai, L., Cheng, Y., Ji, Y., Zhang, F.,
664 Rosenfeld, D., Liss, P. S., Duce, R. A., Kolb, C. E., Molina, M. J.: Persistent sulfate formation from
665 London Fog to Chinese haze, *Proc. Natl. Acad. Sci. U. S. A.*, 113 (48), 13630–13635,
666 <https://doi.org/10.1073/pnas.1616540113>, 2016.

667 Wang, H., Lu, K., Chen, X., Zhu, Q., Chen, Q., Guo, S., Jiang, M., Li, X., Shang, D., Tan, Z., Wu, Y.,
668 Wu, Z., Zou, Q., Zheng, Y., Zeng, L., Zhu, T., Hu, M., Zhang, Y.: High N₂O₅ Concentrations
669 Observed in Urban Beijing: Implications of a Large Nitrate Formation Pathway, *Environ. Sci.*
670 *Technol. Lett.*, 4 (10), 416–420, <https://doi.org/10.1021/acs.estlett.7b00341>, 2017.

671 Wang, T., Nie, W., Gao, J., Xue, L. K., Gao, X. M., Wang, X. F., Qiu, J., Poon, C. N., Meinardi, S.,
672 Blake, D., Wang, S. L., Ding, A. J., Chai, F. H., Zhang, Q. Z., and Wang, W. X.: Air quality during
673 the 2008 Beijing Olympics: secondary pollutants and regional impact, *Atmos. Chem. Phys.*, 10,
674 7603–7615, <https://doi.org/10.5194/acp-10-7603-2010>, 2010.

675 Wang, Y., Zhang, Q., Jiang, J., Zhou, W., Wang, B., He, K., Duan, F., Zhang, Q., Philip, S., and Xie,
676 Y.: Enhanced sulfate formation during China’s severe winter haze episode in January 2013 missing
677 from current models, *J. Geophys. Res.-Atmos.*, 119, 10425– 10440,
678 <https://doi.org/10.1002/2013JD021426>, 2014.

679 Wang Y., Zhang F., Li Z., Tan H., Xu H., Ren J., Zhao J., Du W. and Sun Y.: Enhanced hydrophobicity
680 and volatility of submicron aerosols under severe emission control conditions in Beijing, *Atmos*
681 *Chem Phys*, 17, 5239-5251, <https://doi.org/10.5194/acp-17-5239-2017>, 2017.

682 Wang Y., Li Z., Zhang Y., Du W., Zhang F., Tan H., Xu H., Fan T., Jin X., Fan X., Dong Z., Wang Q.
683 and Sun Y.: Characterization of aerosol hygroscopicity, mixing state, and CCN activity at a suburban
684 site in the central North China Plain, *Atmos. Chem. Phys.*, 18, 11739-11752,
685 <https://doi.org/10.5194/acp-18-11739-2018>, 2018.

686 Wehner, B., Birmili, W., Ditas, F., Wu, Z., Hu, M., Liu, X., Mao, J., Sugimoto, N., and Wiedensohler,
687 A.: Relationships between sub micrometer particulate air pollution and air mass history in Beijing,
688 China, 2004–2006, *Atmos. Chem. Phys.*, 8, 6155–6168, <https://doi.org/10.5194/acp-8-6155-2008>,
689 2008.

690 Wei, J., Huang, W., Li, Z., Xue, W., Peng, Y., Sun, L., and Cribb, M. Estimating 1-km-resolution PM_{2.5}
691 concentrations across China using the space-time random forest approach, *Remote Sensing of*

692 Environment, 231, 1-14. <https://doi.org/10.1016/j.rse.2019.111221>, 2019a.

693 Wei, J., Li, Z., Guo, J., Sun, L., Huang, W., Xue, W., Fan, T., and Cribb, M. Satellite-derived 1-km-
694 resolution PM₁ concentrations from 2014 to 2018 across China, *Environmental Science &*
695 *Technology*. <https://doi.org/10.1021/acs.est.9b03258>, 2019b.

696 Wexler, A.S., Clegg, S.L.: Atmospheric aerosol models for systems including the ions H⁺, NH₄⁺, Na⁺,
697 SO₄²⁻, NO₃⁻, Cl⁻, Br⁻, and H₂O, *J. Geophys. Res.-Atmos.*, 107 (D14): 14-14,
698 <https://doi.org/10.1029/2001JD000451>, 2002.

699 Whitby, K. T.: The physical characteristics of sulfur aerosols, *Atmos. Environ.*, 12, 135–159,
700 <https://doi.org/10.1016/j.atmosenv.2007.10.057>, 1978.

701 Wiedensohler A.: An approximation of the bipolar charge distribution for particles in the submicron
702 size range, *J. Aerosol Sci.*, 19, 387–389, [https://doi.org/10.1016/0021-8502\(88\)90278-9](https://doi.org/10.1016/0021-8502(88)90278-9), 1988.

703 Wu, G. X., Li, Z. Q., Fu, C. B., Zhang, X. Y., Zhang, R. Y., Zhang, R. H., Zhou, T. J., Li, J. P., Li, J.
704 D., and Zhou, D. G.: Advances in studying interactions between aerosols and monsoon in China,
705 *Science China Earth Science*, 59, 1–16, <https://doi.org/10.1007/s11430-015-5198-z>, 2016.

706 Wu, Z., Wang, Y., Tan, T., Zhu, Y., Li, M., & Shang, D., et al.: Aerosol liquid water driven by
707 anthropogenic inorganic salts: implying its key role in the haze formation over north china
708 plain, *Environ. Sci. Technol. Lett.*, 5(3), 160-166, <https://doi.org/10.1021/acs.estlett.8b00021>, 2018.

709 Xu, L., Guo, H., Boyd, C. M., Klein, M., Bougiatioti, A., Cerully, K. M., Hite, J. R., Isaacman-
710 VanWertz, G., Kreisberg, N. M., Knote, C., Olson, K., Koss, A., Goldstein, A. H., Hering, S. V., de
711 Gouw, J., Baumann, K., Lee, S.-H., Nenes, A., Weber, R. J., and Ng, N. L.: Effects of anthropogenic
712 emissions on aerosol formation from isoprene and monoterpenes in the southeastern United States,
713 *P. Natl. Acad. Sci.*, 112, 37–42, <https://doi.org/10.1073/pnas.1417609112>, 2015.

714 Xu, W., Han, T., Du, W., Wang, Q., Chen, C., Zhao, J., Zhang, Y., Li, J., Fu, P., Wang, Z., Worsnop, D.
715 R., Sun, Y.: Effects of Aqueous- Phase and Photochemical Processing on Secondary Organic
716 Aerosol Formation and Evolution in Beijing, China, *Environ. Sci. Technol. Lett.*, 51 (2), 762–770,
717 <https://doi.org/10.1021/acs.est.6b04498>, 2017.

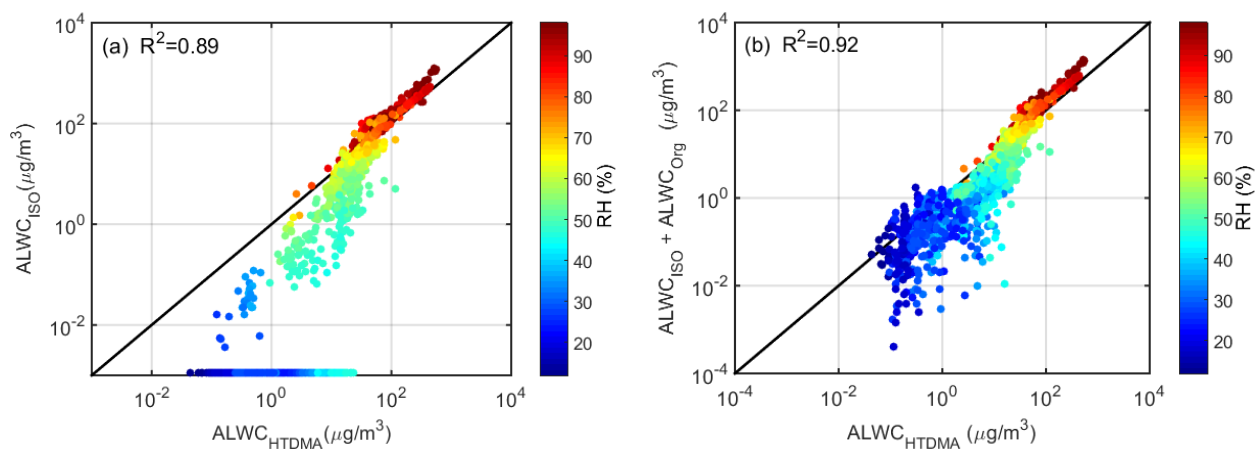
718 Zheng, B., Zhang, Q., Zhang, Y., He, K. B., Wang, K., Zheng, G. J., Duan, F. K., Ma, Y. L., Kimoto,
719 T.: Heterogeneous chemistry: a mechanism missing in current models to explain secondary
720 inorganic aerosol formation during the January 2013 haze episode in North China, *Atmos. Chem.*
721 *Phys.*, 15 (4), 2031–2049, <https://doi.org/10.5194/acp-15-2031-2015>, 2015.

722 Zieger, P., Väisänen, O., Corbin, J. C., Partridge, D. G., Bastelberger, S., Mousavi-Fard, M., Rosati,
723 B., Gysel, M., Krieger, U. K., Leck, C., Nenes, A., Riipinen, I., Virtanen, A., and Salter, M. E.:
724 Revising the hygroscopicity of inorganic sea salt particles, *Nature communications*, 8, 15883,

725 <https://doi.org/10.1038/ncomms15883>, 2017.

726

727



728

729 **Figure 1. Comparison between ALWC_{HTDMA} and (a) ALWC_{ISO} and (b) the sum of ALWC_{ISO} and ALWC_{Org}.**

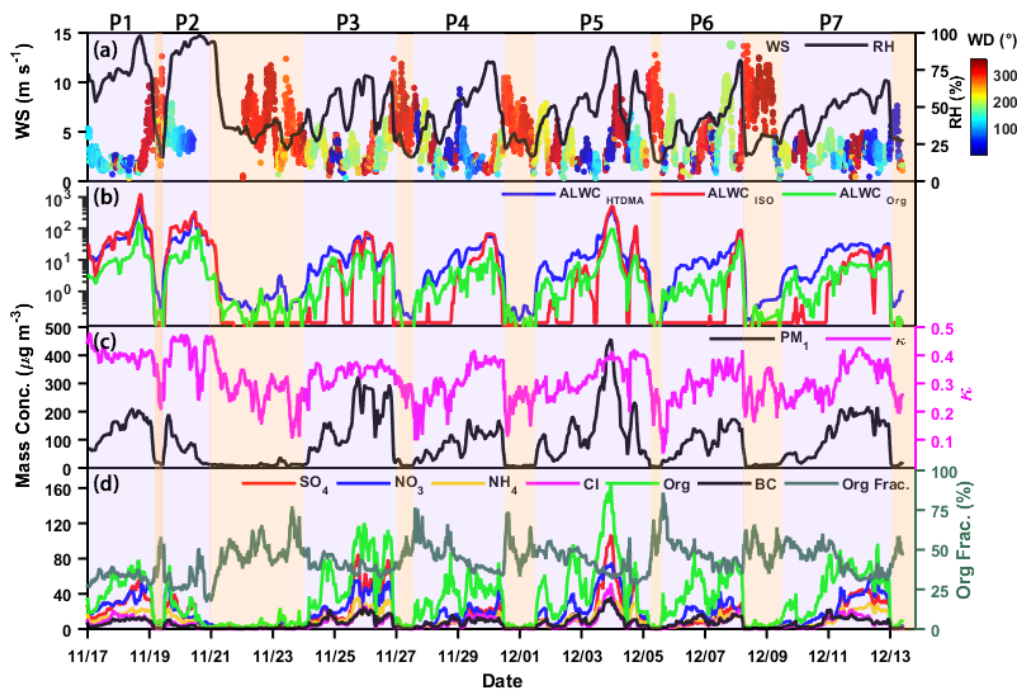
730 ALWC_{HTDMA} refers to calculated ALWC based on the measured growth factor and PNSDs, ALWC_{ISO} refers to

731 simulated ALWC from the ISORROPIA II model, and ALWC_{Org} refers to the inferred ALWC contributed by

732 organic species. The coefficient of determination R² is given in each panel. The color of the dots denotes the ambient

733 RH; the solid line denotes the 1:1 line.

734

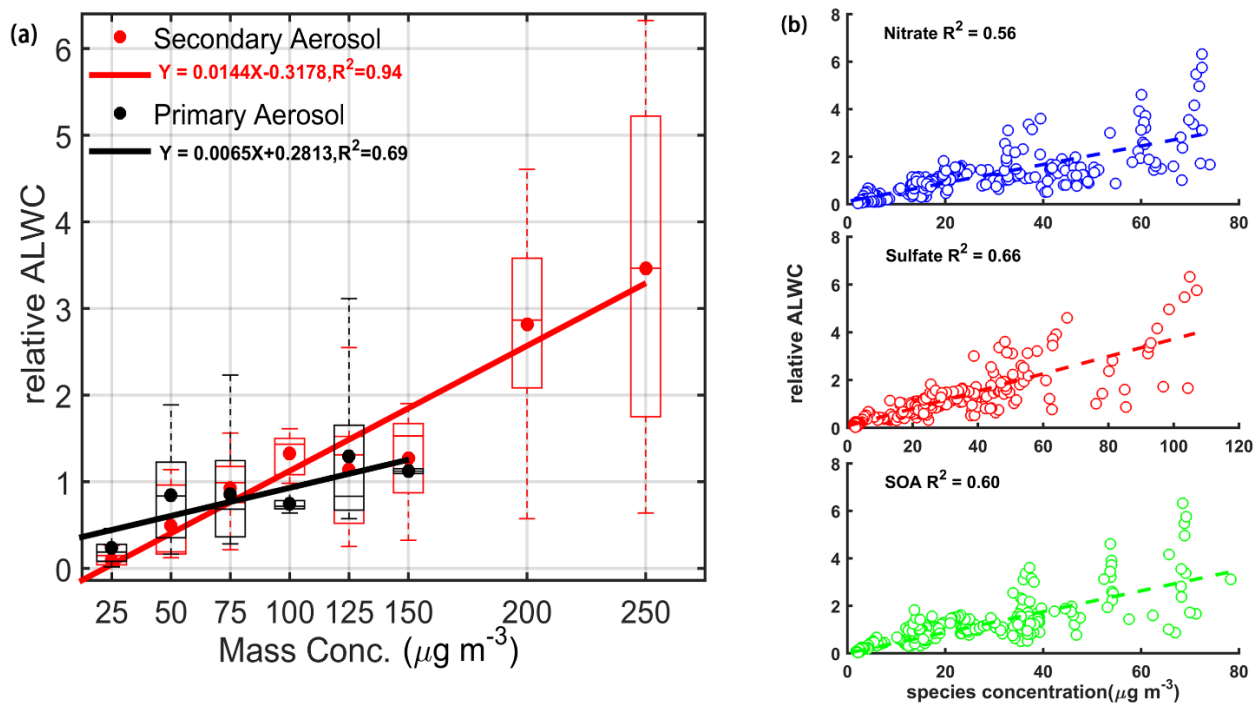


735

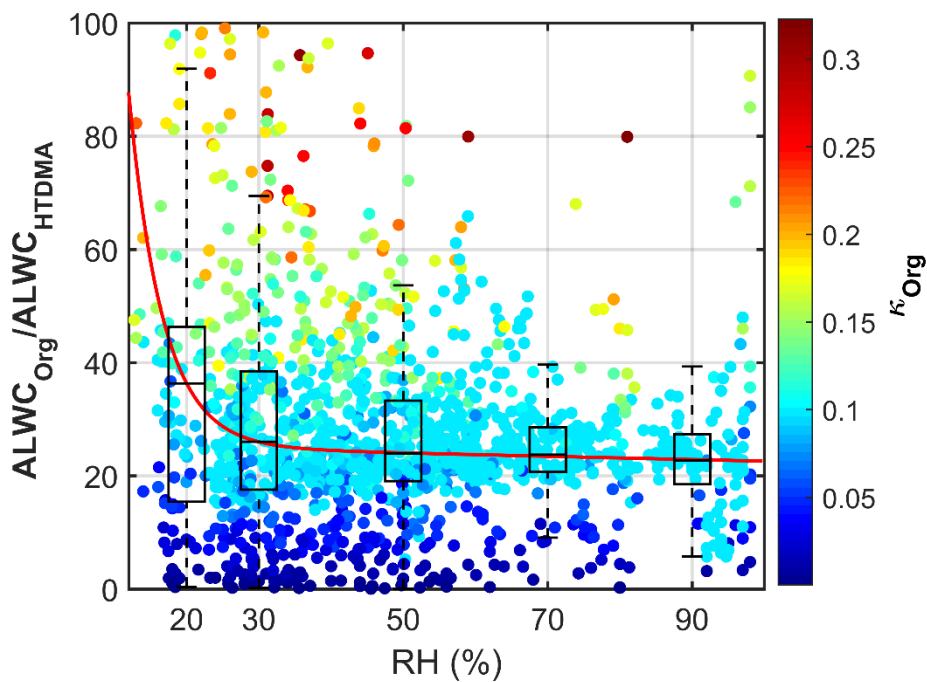
736 **Figure 2. Time series of (a) wind speed (WS, left y-axis), ambient relative humidity (RH, right y-axis), and wind**

737 **direction (WD, colored dots), (b) ALWC_{HTDMA} (in blue), ALWC_{ISO} (in red), and ALWC_{Org} (in green), (c) PM₁ mass**

738 concentration (left y-axis) and hygroscopicity parameter (κ , right y-axis) calculated using the ZSR model described
 739 by Eq. (7), and (d) mass concentrations of aerosol species in PM₁ (left y-axis) and organic aerosol mass fraction
 740 (right y-axis). Seven polluted episodes (segments of the time series with a purple background) are selected for
 741 examination.
 742

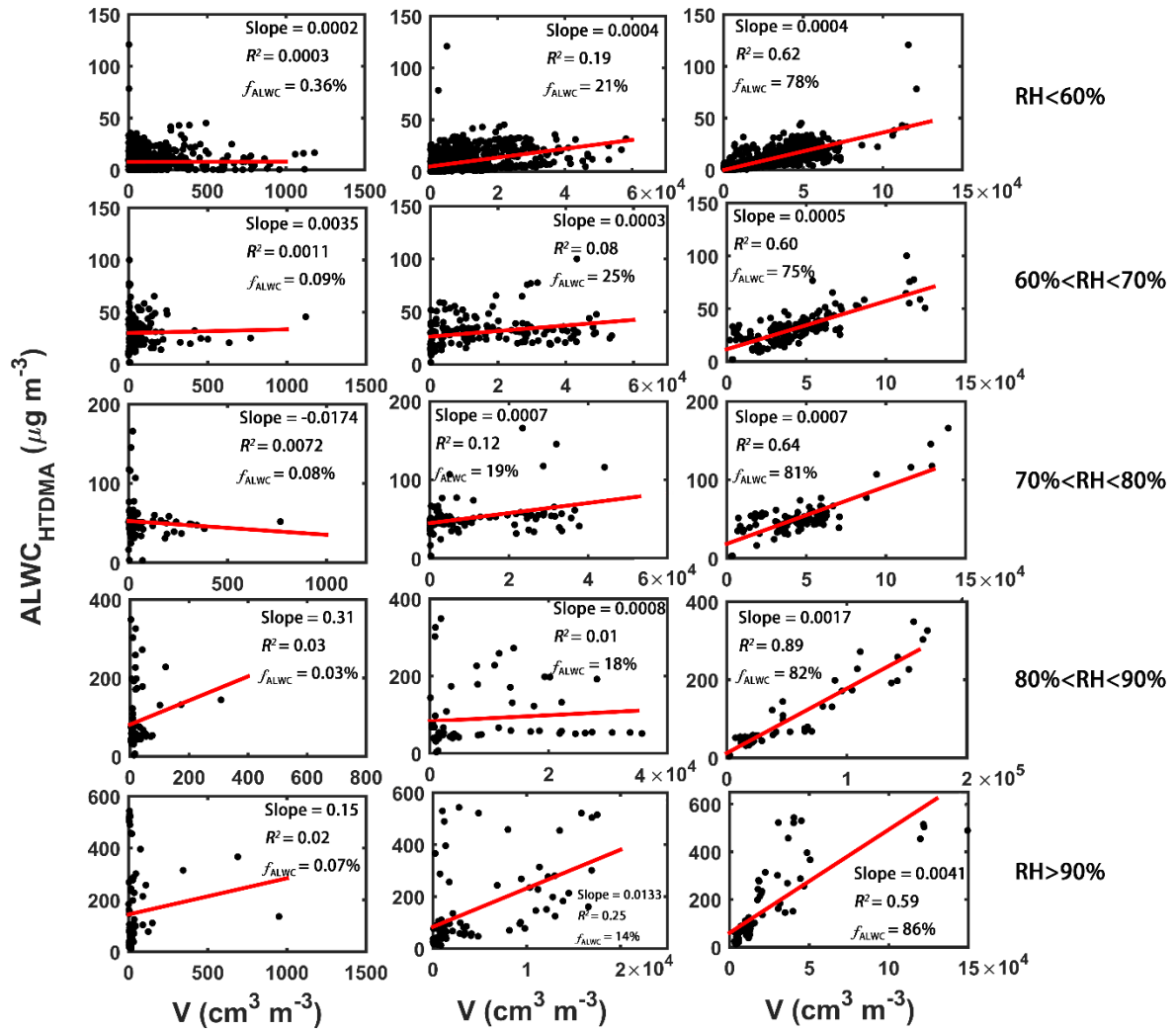


743
 744 **Figure 3. The correlation analysis between relative ALWC and (a) primary (in black) and secondary (in red) aerosol**
 745 **mass concentrations, and (b) nitrate, sulfate, and secondary organic aerosol (SOA) mass concentrations. Panel (a)**
 746 **shows mean relative ALWCs (solid dots) with boxes showing the 25th, 50th, and 75th percentiles. The extremities**
 747 **show the 5th and 95th percentiles. The solid lines in (a) and the dashed lines in (b) both represent the corresponding**
 748 **best-fit lines from linear regression.**



749

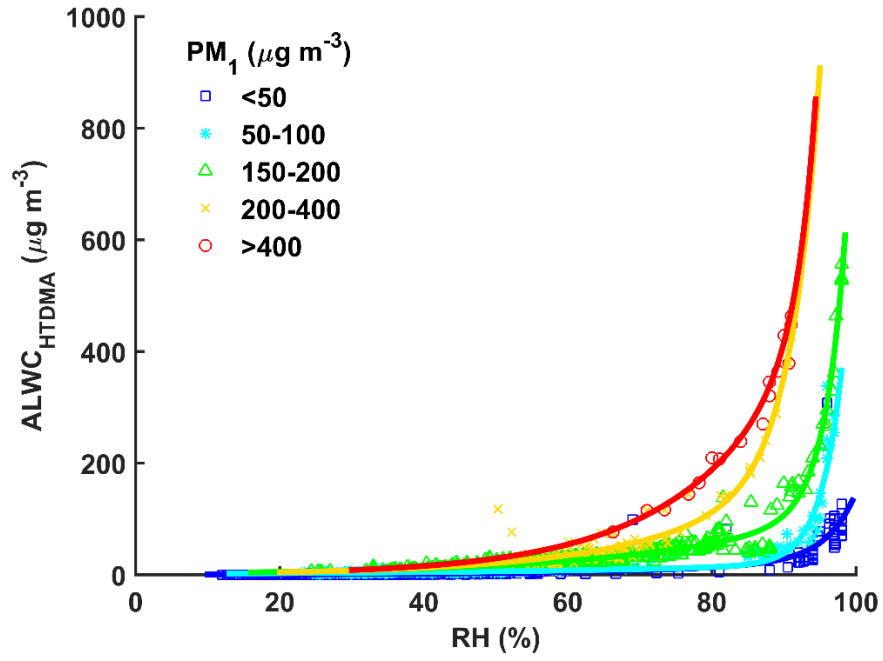
750 **Figure 4.** The variation of the fraction of $ALWC_{Org}$ in total $ALWC$ ($ALWC_{HTDMA}$) with the ambient relative humidity
 751 **(RH).** The color of the dots denotes the hygroscopicity parameter of organics (κ_{Org}). The boxes show the fraction of
 752 $ALWC_{Org}$ with the 25th, 50th, and 75th percentiles. The extremities show the 5th and 95th percentiles. The red line
 753 shows the fitting curve with the function $y = ae^{bx}$.



754

755 **Figure 5.** The correlation analysis between $ALWC_{HTDMA}$ and the volume concentration of nucleation mode (left
 756 column), Aitken mode (middle column), and accumulation mode (right column) particles under different ambient
 757 relative humidity (RH) conditions. The average contribution of each mode particles to ALWC under different
 758 ambient RH conditions is denoted by f_{ALWC} . The red lines represent the best-fit lines from linear regression.

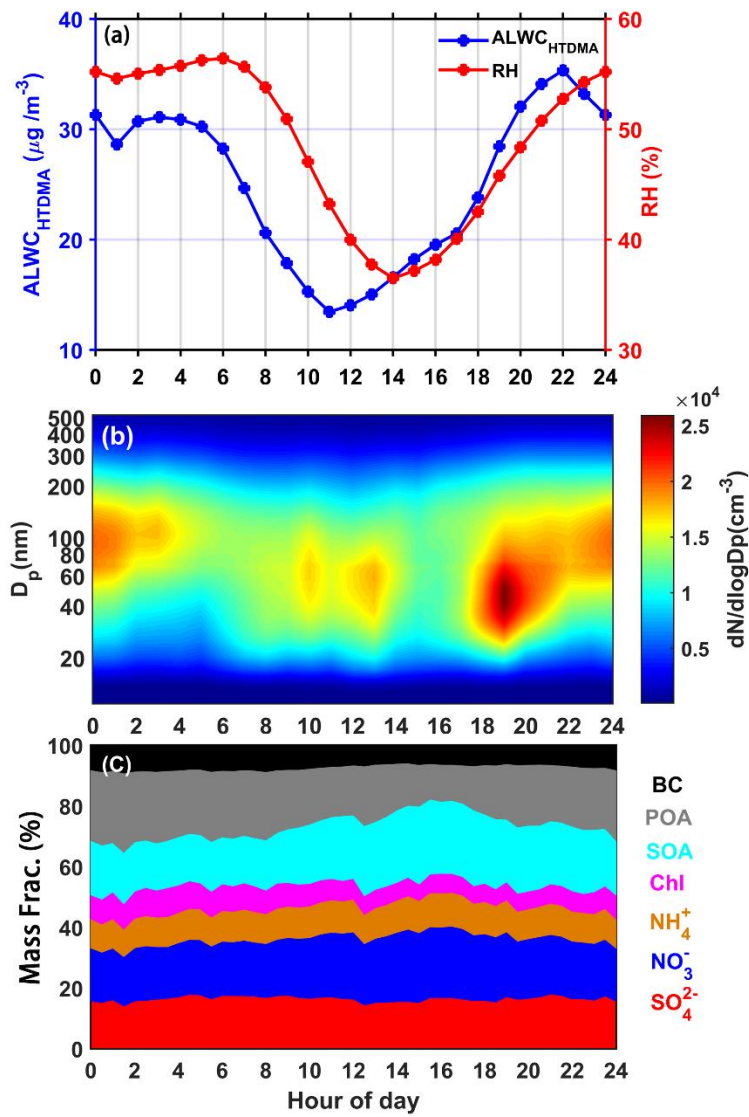
759



760

761 **Figure 6. The dots show how $ALWC_{HTDMA}$ varies with the ambient relative humidity (RH) for different PM_1 mass**
 762 **concentration ranges (colored symbols). The colored curves represent the best-fit lines through the data using the**
 763 **fitting function $y = ae^{bx}$.**

764

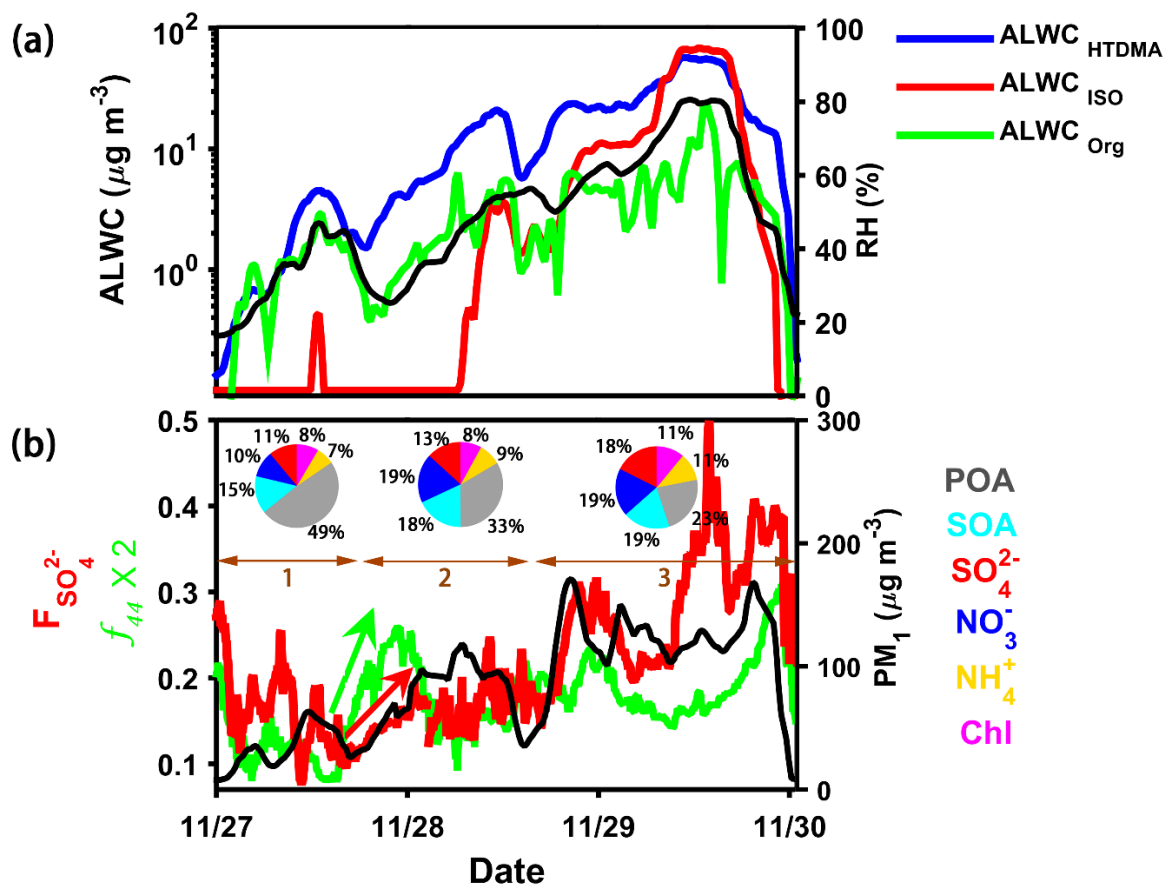


765

766 Figure 7. Diurnal variations of (a) ALWC_{HTDMA} (in blue) and ambient RH (in red), (b) particle number size

767 distribution, and (c) the mass fraction of different chemical species. The time is in Beijing time.

768



769

770 Figure 8. Time series of (a) $\text{ALWC}_{\text{HTDMA}}$ (in blue), ALWC_{ISO} (in red), ALWC_{Org} (in green), and RH (right y-axis), and
 771 (b) the sulfur oxidation ratio ($F_{\text{SO}_4^{2-}}$), f_{44} , and PM_{10} mass concentration (right y-axis) during the P4 case in Figure 2.
 772 The pie charts in (b) represent the average chemical compositions of PM_{10} during three stages of the pollution event
 773 (denoted by brown horizontal lines). The red and green arrows in (b) indicate the rapid increase in $F_{\text{SO}_4^{2-}}$ and f_{44} at
 774 the initial stage.

775